

Hole and electron dynamics in the triangular-lattice antiferromagnet — interplay of frustration and spin fluctuations

Pooja Srivastava* and Avinash Singh†

Department of Physics, Indian Institute of Technology Kanpur - 208016

(Dated: May 11, 2018)

Single-particle dynamics in the 120° ordered antiferromagnetic state of the triangular-lattice Hubbard model is studied using a physically transparent fluctuation approach in terms of multiple magnon emission and absorption processes within the noncrossing approximation. Hole and electron spectral features are evaluated at intermediate U , and analyzed in terms of a competition between the frustration-induced direct hopping and the virtual hopping. Finite U -induced competing interactions and frustration effects contributing through the magnon dispersion are also discussed. Finite contribution to self-energy correction from long-wavelength (Goldstone) modes, together with the high density of electron scattering states in the narrow, sharp peak in the upper band, result in strong fermion-magnon scattering leading to pronounced incoherent behaviour in the electron dynamics. The fluctuation-induced first-order metal-insulator transition due to vanishing band gap is also discussed.

PACS numbers: 71.10.Fd, 75.50.Ee, 75.30.Ds, 75.10.Lp

I. INTRODUCTION

There has been renewed interest in correlated electron systems on triangular lattices, as evidenced by recent studies of antiferromagnetism, superconductivity and metal-insulator transition in the organic systems $\kappa - (\text{BEDT} - \text{TTF})_2\text{X}$,^{1,2} the discovery of superconductivity in $\text{Na}_x\text{CoO}_2 \cdot y\text{H}_2\text{O}$,³ the observation of low-temperature insulating phases in some $\sqrt{3}$ -adlayer structures such as K on Si[111],⁴ and quasi two-dimensional 120° spin ordering and spin-wave excitations in $\text{RbFe}(\text{MoO}_4)_2$ (Refs. 5,6) and the multiferroic material HoMnO_3 .^{7,8}

The recent finding of finite U -induced competing interactions and frustration in the 120° ordered antiferromagnetic (AF) state of the Hubbard model on a triangular lattice,⁹ resulting in vanishing spin stiffness at $U \approx 6$ and a magnetic instability towards a F-AF state at $U \approx 7$, both in the insulating state, adds a new dimension to the intrinsic geometric frustration of the triangular-lattice antiferromagnet. Indeed, strongly enhanced quantum spin fluctuations associated with the magnetic instability may account for the absence of long-range magnetic order in the *nearly isotropic* organic antiferromagnet $\kappa - (\text{BEDT} - \text{TTF})_2\text{Cu}_2(\text{CN})_3$, as inferred from recent ^1H NMR and static susceptibility measurements down to 32 mK, well below the estimated exchange constant $J \sim 250$ K, suggesting the realization of a quantum spin-liquid state.¹⁰ The realization of a non-magnetic insulator at intermediate U is also interesting as it allows, with decreasing U , for a Mott-type metal-insulator transition not accompanied by any magnetic symmetry breaking, as seen in the layered system $\kappa - (\text{BEDT} - \text{TTF})_2\text{Cu}[\text{N}(\text{CN})_2]\text{Cl}$,¹¹ and currently of much theoretical interest.^{12,13}

Recently, self-energy corrections due to multiple magnon processes in the AF state of the frustrated square-lattice $t - t'$ -Hubbard model were evaluated using a fluctuation approach.¹⁴ Quasiparticle dispersion

obtained with the same set of Hubbard model cuprate parameters as obtained from a recent magnon spectrum fit¹⁵ was found to yield excellent agreement with ARPES data for $\text{Sr}_2\text{CuO}_2\text{Cl}_2$,¹⁴ thus providing a unified description of magnetic and electronic excitations in cuprates.

It is therefore interesting to examine and contrast self-energy corrections and quasiparticle behaviour in the 120° ordered AF state of the triangular-lattice Hubbard model which involves non-collinear ordering, intrinsic geometric frustration, and also finite U -induced competing interactions and frustration. Indeed, we find that long-wavelength magnon modes yield finite contribution to the fermion-magnon scattering process, unlike the square-lattice case where this contribution was negligible.¹⁴

Frustration and spin fluctuations are involved in an interesting interplay with respect to quasiparticle behaviour. As neighbouring spins are not antiparallel in triangular-lattice and frustrated square-lattice AF states, frustration results in an $O(t)$ or $O(t')$ direct hopping in addition to the $O(J)$ virtual hopping. Competition between the two dispersions results in band broadening/narrowing, which has a dramatic effect on self-energy corrections due to significantly different density of fermion scattering states. Competition also results in a reduced band gap, thus bringing the system closer to a metal-insulator (MI) transition. The $t - J$ model calculations do not involve this competition as the virtual hopping term is absent.

In this paper, we examine the hole and electron spectral functions in terms of self-energy corrections in the 120° ordered AF state of the Hubbard model on a triangular lattice. Hole and electron dynamics in an antiferromagnetic background is associated with multiple magnon emission and absorption processes corresponding to broken AF bonds, string states, and scrambling of the AF spin ordering. The fluctuation approach adopted in this paper in terms of a diagrammatical expansion provides a physically transparent picture in which the hole

motion is renormalized due to the fluctuating transverse field associated with spin fluctuations. This fluctuation perspective is physically relevant in view of the substantial ordered-moment reduction, which approaches 59% in the strong-coupling (Heisenberg) limit.¹⁶

Single-particle dynamics in the AF state of the triangular-lattice $t - J$ model has been studied in the self-consistent Born approximation (SCBA),^{17,18,19} exact diagonalization,¹⁷ and projection techniques.^{20,21} One-electron density of states has been examined using the quantum Monte Carlo method,²² showing a pseudogap development for intermediate U .

We consider the Hubbard model

$$\mathcal{H} = -t \sum_{i\delta\sigma} a_{i,\sigma}^\dagger a_{i+\delta,\sigma} + U \sum_i a_{i\uparrow}^\dagger a_{i\uparrow} a_{i\downarrow}^\dagger a_{i\downarrow} \quad (1)$$

with nearest-neighbour (NN) hopping on a triangular lattice. The model has particle-hole symmetry under the transformation $t \rightarrow -t$. In this paper we consider the case of positive t and hole (electron) doping in the lower (upper) band; same result holds for negative t and electron (hole) doping in the upper (lower) band. In the following we set the hopping energy $t = 1$.

The organization of this paper is as follows. The three-sublattice basis is briefly reviewed in section II to introduce the notation and key features of the classical-level fermion dispersion. Transverse spin fluctuations are introduced in section III in terms of magnon amplitudes and energies. Intraband self-energy corrections due to multi-magnon processes are studied in section IV in the non-crossing approximation. Hole and electron spectral functions for the lower and upper bands are discussed in section V and conclusions are presented in section VI.

II. THREE-SUBLATTICE REPRESENTATION

While the spiral-state description applies only to Bravais lattices, the sublattice-basis description applies to Kagomé type non-Bravais lattices as well. In general, the 120° AF state is characterized by an ordering plane (normal \hat{n}_1) and a planar direction (\hat{n}_2) in spin space, with reference to which spin orientations are given by

$$\hat{\alpha} = \cos \phi_\alpha \hat{n}_2 + \sin \phi_\alpha (\hat{n}_1 \times \hat{n}_2) \quad (2)$$

corresponding to angles $\phi_\alpha = 0^\circ, 120^\circ$, and 240° on the three sublattices $\alpha = A, B, C$. A convenient choice is $\hat{n}_1 = \hat{z}$ (spin-ordering in the $x - y$ plane) and $\hat{n}_2 = \hat{x}$, so that the local mean field $\Delta_\alpha = \frac{1}{2} U \langle \Psi_i^\dagger \boldsymbol{\sigma} \Psi_i \rangle_\alpha$ in the 120° ordered Hartree-Fock state is given by

$$\Delta_\alpha = \Delta \hat{\alpha} \quad (\hat{\alpha} = \hat{a}, \hat{b}, \hat{c}) \quad (3)$$

on the three sublattices in terms of the three lattice unit vectors

$$\hat{a} = \hat{x}, \quad \hat{b} = -\frac{1}{2}\hat{x} + \frac{\sqrt{3}}{2}\hat{y}, \quad \hat{c} = -\frac{1}{2}\hat{x} - \frac{\sqrt{3}}{2}\hat{y}. \quad (4)$$

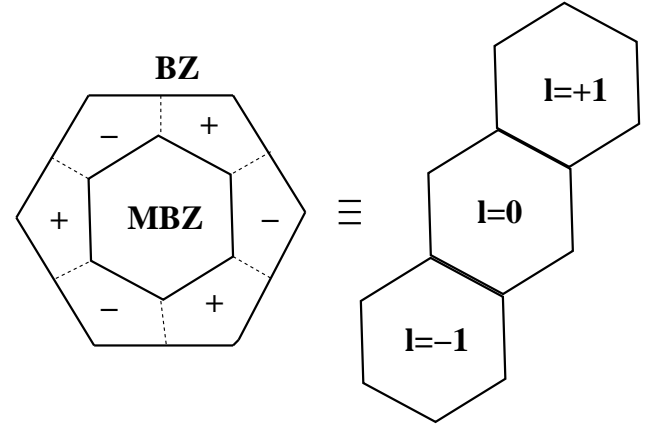


FIG. 1: Brillouin zone (BZ) for the triangular lattice and magnetic Brillouin zone (MBZ) for the 120° ordered AF state, along with the BZ - MBZ correspondence involving the branch index l .

Fourier transformation within the sublattice basis yields

$$\mathcal{H}_{\text{HF}} = \sum_{\mathbf{k}} \Psi_{\mathbf{k}}^\dagger \begin{bmatrix} -\boldsymbol{\sigma} \cdot \Delta_A & \delta_{\mathbf{k}} & \delta_{\mathbf{k}}^* \\ \delta_{\mathbf{k}}^* & -\boldsymbol{\sigma} \cdot \Delta_B & \delta_{\mathbf{k}} \\ \delta_{\mathbf{k}} & \delta_{\mathbf{k}}^* & -\boldsymbol{\sigma} \cdot \Delta_C \end{bmatrix} \Psi_{\mathbf{k}}, \quad (5)$$

where $\Psi_{\mathbf{k}} \equiv (a_{\mathbf{k}\uparrow} \ a_{\mathbf{k}\downarrow} \ b_{\mathbf{k}\uparrow} \ b_{\mathbf{k}\downarrow} \ c_{\mathbf{k}\uparrow} \ c_{\mathbf{k}\downarrow})$ in terms of the fermion operators $a_{\mathbf{k}}, b_{\mathbf{k}}, c_{\mathbf{k}}$ defined on the three sublattices A, B, C. Wavevector \mathbf{k} lies within the Magnetic Brillouin Zone (MBZ), corresponding to the three inter-penetrating triangular sublattices (lattice parameter $\sqrt{3}a$). The NN hopping term

$$\delta_{\mathbf{k}} = -t \sum_{\hat{\delta}=\hat{a},\hat{b},\hat{c}} e^{i\mathbf{k} \cdot \hat{\delta}} = -t[e^{ik_x} + 2e^{-ik_x/2} \cos(\sqrt{3}k_y/2)] \quad (6)$$

mixes AB, BC, and CA sublattices, which are connected by the three lattice unit vectors. The lattice hopping term $\delta_{\mathbf{k}}$ yields the triangular-lattice free-fermion energy

$$\epsilon_{\mathbf{k}} = \delta_{\mathbf{k}} + \delta_{\mathbf{k}}^* \quad (7)$$

and transforms as

$$\delta_{\mathbf{k} \pm \mathbf{Q}} = \delta_{\mathbf{k}} e^{\pm i2\pi/3} \quad (8)$$

under momentum translation by the ordering wavevector $\mathbf{Q} = (2\pi/3, 2\pi/\sqrt{3})$.

The $[6 \times 6]$ Hamiltonian matrix obeys the cyclic property $[\mathcal{H}_{\text{HF}}]_{AB} = [\mathcal{H}_{\text{HF}}]_{BC} = [\mathcal{H}_{\text{HF}}]_{CA}$ of the 120° ordered state, resulting in the following spin-sublattice structure of the normalized eigenvectors

$$|\mathbf{k}, l\rangle = \frac{1}{\sqrt{3}} \begin{pmatrix} \alpha_{\mathbf{k},l} e^{-i\phi_\alpha} \\ \beta_{\mathbf{k},l} \end{pmatrix}_\sigma \otimes \begin{pmatrix} 1 \\ e^{i\theta_l} \\ e^{-i\theta_l} \end{pmatrix}_\alpha, \quad (9)$$

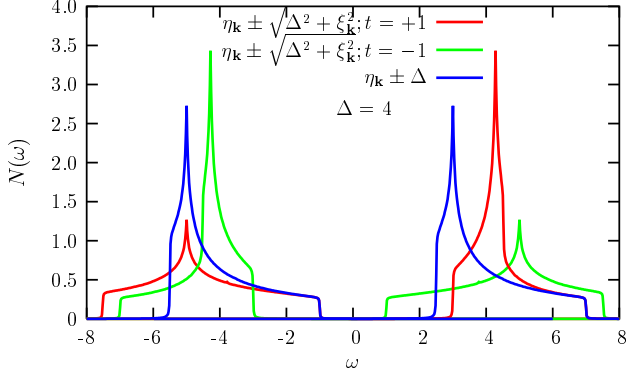


FIG. 2: (color online) Comparison of density of states corresponding to the full HF dispersion and the direct hopping dispersion, showing the band broadening (narrowing) due to the virtual hopping dispersion.

where the planar spin orientations $\phi_\alpha = 0^\circ, 120^\circ, 240^\circ$ for the three sublattices, and the sublattice phase angle $\theta_l = 2\pi l/3$ for the three fermion branches $l = 0, \pm 1$. Substituting the above eigenvector structure, and contracting over the sublattice sector α , the eigenvalue equations of the $[6 \times 6]$ Hamiltonian matrix reduce to three $[2 \times 2]$ equations in the spin sector corresponding to $l = 0, \pm 1$; the six eigenvalues $E_{\mathbf{k},l}^\mp$ and amplitudes $(\alpha_{\mathbf{k},l}^\mp, \beta_{\mathbf{k},l}^\mp)$ for the lower (-) and upper (+) AF bands are then given by

$$E_{\mathbf{k},l}^\mp = \eta_{\mathbf{k}} \pm \sqrt{\Delta^2 + \xi_{\mathbf{k}}^2} \quad (10)$$

$$\alpha_{\mathbf{k},l}^\mp = \pm \frac{1}{\sqrt{2}} \left(1 \pm \frac{\xi_{\mathbf{k}}}{\sqrt{\Delta^2 + \xi_{\mathbf{k}}^2}} \right)^{1/2} \quad (11)$$

$$\beta_{\mathbf{k},l}^\mp = + \frac{1}{\sqrt{2}} \left(1 \mp \frac{\xi_{\mathbf{k}}}{\sqrt{\Delta^2 + \xi_{\mathbf{k}}^2}} \right)^{1/2},$$

where $\eta_{\mathbf{k}} \equiv (\epsilon_{\mathbf{k}} + \epsilon_{\mathbf{k}-\mathbf{Q}})/2$ and $\xi_{\mathbf{k}} \equiv (\epsilon_{\mathbf{k}} - \epsilon_{\mathbf{k}-\mathbf{Q}})/2$, with momentum values $\mathbf{k}, \mathbf{k} \pm \mathbf{Q}$ corresponding to fermion branches $l = 0, \pm 1$, respectively. The mean field Δ and magnetization m are related to U through the self-consistency condition.⁹

Typical of the AF state, upper band states yield a negative contribution to spin densities due to the negative sign of $\alpha_{\mathbf{k}}^+$. Consequently, when the two bands start overlapping on decreasing U , partial occupation of the upper band has an amplified effect on reduction of magnetic order — reduced sublattice magnetization due to band overlap decreases the mean-field Δ , which further increases the overlap. Typically, the magnetic order therefore falls very rapidly after band overlap sets in.

The density of states (DOS) corresponding to the full HF (classical) dispersion in Eq. (10), shown in Fig. 2 for both positive and negative t , exhibits a key competition between the two dispersion terms associated with direct hopping ($\eta_{\mathbf{k}}$) of order t and virtual hopping ($\sqrt{\Delta^2 + \xi_{\mathbf{k}}^2} - \Delta$), which is of order J in the strong-coupling limit. For positive t , both dispersion terms favour same state at the

top of the lower band, while they favour different states at the bottom of the upper band, thereby causing band narrowing. The competition results in broadening and narrowing of the lower and upper bands, depending on the sign of t , which has a dramatic effect on the self-energy correction due to significantly different density of fermion scattering states. There is no such competition in the $t - J$ model studies where the virtual hopping dispersion term is absent.

From Eq. (8), it follows that

$$\epsilon_{\mathbf{k}} = -(\epsilon_{\mathbf{k}+\mathbf{Q}} + \epsilon_{\mathbf{k}-\mathbf{Q}}) \quad (12)$$

so that

$$\eta_{\mathbf{k}-\mathbf{Q}} = -\frac{\epsilon_{\mathbf{k}}}{2}. \quad (13)$$

Therefore, the direct hopping dispersion $\eta_{\mathbf{k}-\mathbf{Q}}$, to which the HF quasiparticle dispersion (10) reduces in the strong-coupling limit, is identical to the classical-level dispersion $\epsilon_{\mathbf{k}}/2$ taken in earlier $t - J$ model studies, corresponding to effective hopping $t \cos(120^\circ) = -t/2$ associated with the 120° ordering, where momentum translation by \mathbf{Q} connects the real and slave fermions.¹⁷ Comparison of DOS corresponding to the full dispersion with that of $\eta_{\mathbf{k}}$ is also shown in Fig. 2.

III. TRANSVERSE SPIN FLUCTUATIONS

Including both transverse and longitudinal spin fluctuations, the full spin-fluctuation propagator $\langle \Psi_G | T[S_i^\mu(t) S_j^\nu(t')] | \Psi_G \rangle$ in the 120° ordered AF state has been studied recently in the random phase approximation (RPA) in the full U range.⁹ Even in the intermediate-coupling regime, the magnitude of longitudinal fluctuation $\langle S_\alpha^2 \rangle$ along the local ordering directions $\hat{\alpha}$ was found to be quite negligible ($\langle S_\alpha^2 \rangle \sim 10^{-4}$ at $U \approx 7$). We therefore focus on transverse spin fluctuations along the two locally normal spin directions.

Spin rotation about the \hat{z} direction

$$\begin{pmatrix} \sigma_x \\ \sigma_y \\ \sigma_z \end{pmatrix}' = \begin{bmatrix} \cos \phi_\alpha & \sin \phi_\alpha & 0 \\ -\sin \phi_\alpha & \cos \phi_\alpha & 0 \\ 0 & 0 & 1 \end{bmatrix} \begin{pmatrix} \sigma_x \\ \sigma_y \\ \sigma_z \end{pmatrix} \quad (14)$$

by angles $\phi_\alpha = 0^\circ, 120^\circ, -120^\circ$ for $\alpha = A, B, C$ renders x' as the spin ordering direction for all three sublattices. In the $2 \otimes 3$ spin-sublattice basis of the two transverse spin directions $\mu, \nu = y', z'$ and the three sublattices $\alpha, \beta = A, B, C$, the RPA-level spin-fluctuation propagator is then given by

$$[\chi(\mathbf{q}, \omega)]_{\alpha\beta}^{\mu\nu} = \frac{\frac{1}{2} [\chi^0(\mathbf{q}, \omega)]}{1 - U [\chi^0(\mathbf{q}, \omega)]}, \quad (15)$$

where the bare particle-hole propagator

$$[\chi^0(\mathbf{q}, \omega)]_{\alpha\beta}^{\mu\nu} = \frac{1}{2} \sum_{\mathbf{k}, l, m} \left[\frac{\langle \sigma_\mu \rangle_\alpha^{+-} \langle \sigma_\nu \rangle_\beta^{+*}}{E_{\mathbf{k}-\mathbf{q}, m}^+ - E_{\mathbf{k}, l}^- + \omega} + \frac{\langle \sigma_\mu \rangle_\alpha^{+-} \langle \sigma_\nu \rangle_\beta^{+-*}}{E_{\mathbf{k}, m}^+ - E_{\mathbf{k}-\mathbf{q}, l}^- - \omega} \right] \quad (16)$$

involves integrating out the fermions in the broken-symmetry state. In the particle-hole matrix elements of the rotated spins

$$\langle \sigma_\mu \rangle_\alpha^{-+} \equiv \langle \mathbf{k} - \mathbf{q}, m | \sigma_\mu | \mathbf{k}, l \rangle_\alpha \quad (17)$$

the spin orientation angles ϕ_α in the fermion states (Eq. 9) are transformed out.

We now discuss the spin-sublattice structure of the $[\chi^0(\mathbf{q}, \omega)]$ matrix and its eigenvectors. While the spin-diagonal blocks $[\chi^0(\mathbf{q}, \omega)]^{\mu\mu}$ are Hermitian and the off-diagonal blocks $[\chi^0(\mathbf{q}, \omega)]^{\mu\bar{\mu}}$ are anti-Hermitian, they obey the cyclic symmetry $[\chi^0(\mathbf{q}, \omega)]_{AB} = [\chi^0(\mathbf{q}, \omega)]_{BC} = [\chi^0(\mathbf{q}, \omega)]_{CA}$ of the 120° ordered phase. Also, the sublattice diagonal elements $[\chi^0(\mathbf{q}, \omega)]_{\alpha\alpha}$ are all identical due to sublattice symmetry. Consequently, the normalized eigenvectors of $[\chi^0(\mathbf{q}, \omega)]$ have the following spin-sublattice structure

$$|\phi_\lambda\rangle = \frac{1}{\sqrt{3}} \begin{pmatrix} -iu \\ v \end{pmatrix}_\mu \otimes \begin{pmatrix} 1 \\ e^{i2\pi\lambda/3} \\ e^{-i2\pi\lambda/3} \end{pmatrix}_\alpha \quad (18)$$

where $\lambda = 0, \pm 1$ for the three magnon branches, and the real and normalized amplitudes u and v represent the fluctuation amplitudes in the y' and z' directions, respectively. Contracting over the sublattice index, the eigenvalue equation for $|\phi\rangle$ therefore reduces to

$$[\chi^0(\mathbf{q}, \omega)]|\phi\rangle_\lambda = [\chi_\lambda^0(\mathbf{q}, \omega)] \begin{pmatrix} u \\ v \end{pmatrix} = \lambda_{\mathbf{q}} \begin{pmatrix} u \\ v \end{pmatrix}, \quad (19)$$

where $[\chi_\lambda^0(\mathbf{q}, \omega)]$ is a $[2 \times 2]$ real-symmetric matrix.

Solving the pole equation $1 - U\lambda_{\mathbf{q}}(\omega) = 0$ for the magnon energy $\omega_{\mathbf{q}}$, and expanding $\lambda_{\mathbf{q}}(\omega)$ around the poles to obtain the magnon amplitudes, yields the magnon propagator

$$[\chi(\mathbf{q}, \omega)] = \sum_{\lambda=0,\pm 1} \left[\frac{|\mathbf{q}, \lambda\rangle\langle \mathbf{q}, \lambda|_A}{\omega + \omega_{\mathbf{q}, \lambda} - i\eta} - \frac{|\mathbf{q}, \lambda\rangle\langle \mathbf{q}, \lambda|_R}{\omega - \omega_{\mathbf{q}, \lambda} + i\eta} \right], \quad (20)$$

where the magnon eigenvectors for the advanced (A) and retarded (R) modes are given by

$$|\mathbf{q}, \lambda\rangle = \frac{1}{\sqrt{3}} \begin{pmatrix} \mp i\mathcal{Y}_{\mathbf{q}, \lambda} \\ \mathcal{Z}_{\mathbf{q}, \lambda} \end{pmatrix}_\mu \otimes \begin{pmatrix} 1 \\ e^{i2\pi\lambda/3} \\ e^{-i2\pi\lambda/3} \end{pmatrix}_\alpha \quad (21)$$

in terms of the magnon amplitudes

$$\begin{aligned} \mathcal{Y}_{\mathbf{q}, \lambda} &= u_{\mathbf{q}, \lambda} / \sqrt{2U^2 |d\lambda_{\mathbf{q}, \lambda}/d\omega|} \quad \text{and} \\ \mathcal{Z}_{\mathbf{q}, \lambda} &= v_{\mathbf{q}, \lambda} / \sqrt{2U^2 |d\lambda_{\mathbf{q}, \lambda}/d\omega|} \end{aligned} \quad (22)$$

in the y' and z' directions. Expressions for magnon energy and amplitudes in the strong-coupling limit are given in the Appendix.

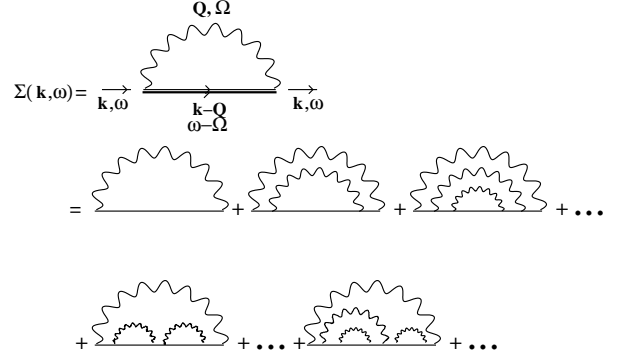


FIG. 3: Self energy in the noncrossing approximation. Wavy lines represent the magnon propagator. The bare fermion-magnon interaction vertex is U .

IV. SELF-ENERGY CORRECTION

Due to multiple magnon emission and absorption processes associated with fermion motion in the AF state, the fermion self energy matrix in the spin-sublattice basis is obtained as

$$\begin{aligned} & [\Sigma(\mathbf{k}, l, \omega)]_{\alpha\beta} \\ &= U^2 \int \frac{d\Omega}{2\pi i} \sum_{\mu\nu} [\sigma_\mu] [G_{\alpha\beta}(\mathbf{k} - \mathbf{q}, m, \omega - \Omega)] [\sigma_\nu] [\chi(\mathbf{q}, \Omega)]_{\alpha\beta}^{\mu\nu} \end{aligned} \quad (23)$$

in the non-crossing (rainbow) approximation.

We consider the intraband contribution involving hole (electron) scattering states in the lower (upper) band, which redistributes the spectral function, leaving the integrated spectral weight and the sublattice magnetization unchanged. We obtain for the hole self energy

$$\begin{aligned} \Sigma_{\mathbf{k}, l}(\omega) &\equiv \langle \mathbf{k}, l | [\Sigma(\mathbf{k}, l, \omega)] | \mathbf{k}, l \rangle \\ &= \sum_{\mathbf{q}, m, \lambda} \frac{|M|^2}{\omega + \omega_{\mathbf{q}, \lambda} - E_{\mathbf{k}-\mathbf{q}, m}^- - \Sigma_{\mathbf{k}-\mathbf{q}, m}(\omega + \omega_{\mathbf{q}, \lambda})} \end{aligned} \quad (24)$$

where the fermion-magnon scattering matrix element

$$M = U \sum_{\alpha\mu} \langle \mathbf{k}, l | \sigma_\mu | \mathbf{k} - \mathbf{q}, m \rangle_\alpha \otimes |\mathbf{q}, \lambda\rangle_{\alpha\mu}^A \quad (25)$$

involves the advanced magnon mode. Substituting the sublattice structure of the fermion and magnon amplitudes, the sum over sublattice index α yields

$$1 + e^{i(m+\lambda-l)2\pi/3} + e^{-i(m+\lambda-l)2\pi/3} = 3 \delta_{m+\lambda-l} \quad (26)$$

effectively amounting to a conservation of sublattice polarization at the fermion-magnon interaction vertex. Therefore, the fermion-magnon scattering matrix element reduces to a sum of the y' and z' fluctuation terms

$$\begin{aligned} M &= \frac{U}{\sqrt{3}} [- (\alpha_{\mathbf{k}, l}^- \beta_{\mathbf{k}-\mathbf{q}, m}^- - \beta_{\mathbf{k}, l}^- \alpha_{\mathbf{k}-\mathbf{q}, m}^-) \mathcal{Y}_{\mathbf{q}, \lambda} \\ &\quad + (\alpha_{\mathbf{k}, l}^- \alpha_{\mathbf{k}-\mathbf{q}, m}^- - \beta_{\mathbf{k}, l}^- \beta_{\mathbf{k}-\mathbf{q}, m}^-) \mathcal{Z}_{\mathbf{q}, \lambda}]. \end{aligned} \quad (27)$$

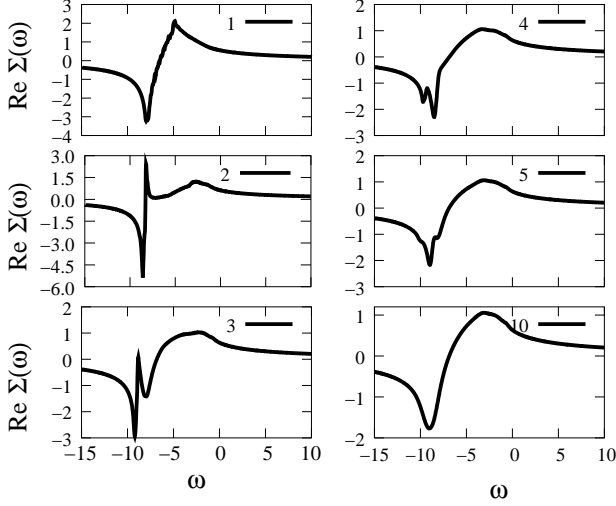


FIG. 4: Variation of hole self energy with iterations, effectively illustrating the role of successively higher-order magnon processes. Here $\Delta = 4$ ($U = 8.8$) and $\mathbf{k} = 0$, $l = -1$.

For fermion and magnon states in the matrix element M , the sublattice-basis MBZ description of momentum translates to a BZ description according to the correspondence $\mathbf{k}, l \rightarrow \mathbf{k} + l\mathbf{Q}$ and $\mathbf{q}, \lambda \rightarrow \mathbf{q} + \lambda\mathbf{Q}$. With this equivalence, Eq. (26) simply corresponds to momentum conservation in the BZ. Analysis of the fermion-magnon matrix element M in the strong-coupling limit and comparison with earlier results for the t - J model is discussed in the Appendix.

It is important to note here that long-wavelength magnon modes yield finite contribution to the fermion-magnon scattering process in the triangular-lattice AF, unlike the square-lattice case where this contribution is negligible.¹⁴ For the square-lattice AF, the small- q contribution was suppressed because the fermion-magnon matrix element $M^2 \sim q$ due to destructive interference within sublattice summation. For the triangular lattice also, for $q = 0$ and $\lambda = 0$ (in-plane mode), the fermion matrix element in Eq. (25) reduces to an expectation value which identically vanishes for $\mu = y'$ as the spins are oriented in the x' direction, yielding similar $M^2 \sim q$ behaviour for small q . However, for the out-of-plane z' fluctuation modes ($\lambda = \pm 1$), the fermion matrix element is finite, resulting in $M^2 \sim 1/q$ and a finite contribution of long-wavelength modes within the two-dimensional ($\int q dq$) momentum summation.

V. RESULTS AND DISCUSSION

The self-consistent numerical evaluation of the self energy (24) was carried out on a 30×40 grid in the MBZ \mathbf{k} space and a frequency interval $\Delta\omega = 0.025$ for ω in the range $-15 < \omega < 10$. The self energy was iteratively evaluated, starting with $\Sigma_{\mathbf{k}}(\omega) = 0$. Typically, self-consistency was achieved within ten iterations for the

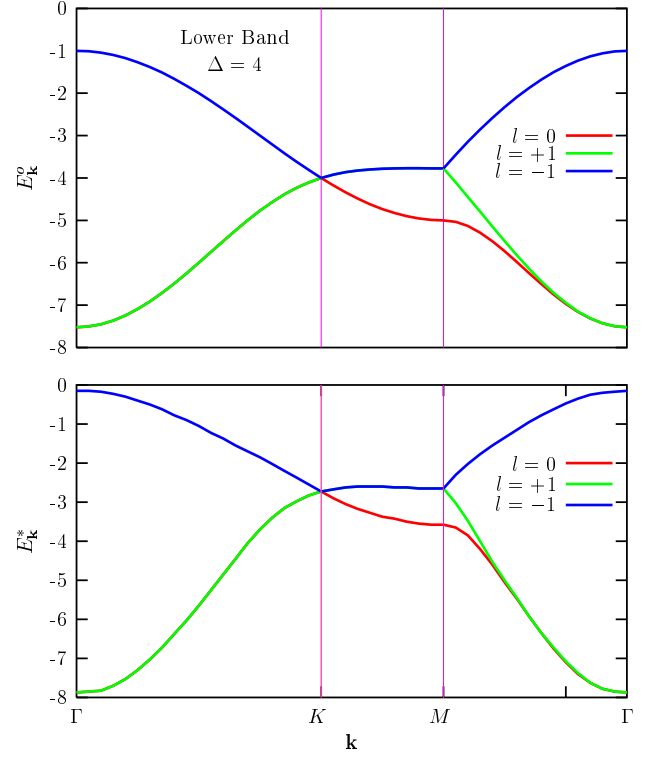


FIG. 5: (color online) Quasiparticle dispersion $E_{\mathbf{k}}^*$ along different symmetry directions in the MBZ (lower panel), along with the HF dispersion $E_{\mathbf{k}}^0$ for comparison (upper panel).

lower band (Fig. 4) and fifteen iterations for the upper band (Fig. 8).

Self-energy corrections for an added hole in the broad, flat band near the top of the lower band are qualitatively different from that of an added electron in the narrow, sharp peak near the bottom of the upper band. The low density of hole scattering states and the dominant band-energy denominator suppresses the hole self energy. However, the electron self energy is significantly enhanced due to the sharp peak and the small band energy compared with magnon energy, resulting in the characteristic signature of string states associated with multi-magnon processes. It is convenient to visualize these qualitatively different self-energy corrections in terms of hole (electron) motion in an effective ferromagnetic (antiferromagnetic) spin background projected out of the 120° spin ordering.

A. Hole Dynamics (Lower Band)

Figure 5 shows renormalized quasiparticle dispersion along different symmetry directions in the MBZ. Comparison with the HF result shows nearly momentum independent shift in the quasiparticle energies, leaving the effective hole mass essentially unchanged. States in upper portion of the band are pushed up, while those in the lower portion are pulled down, in accordance with the

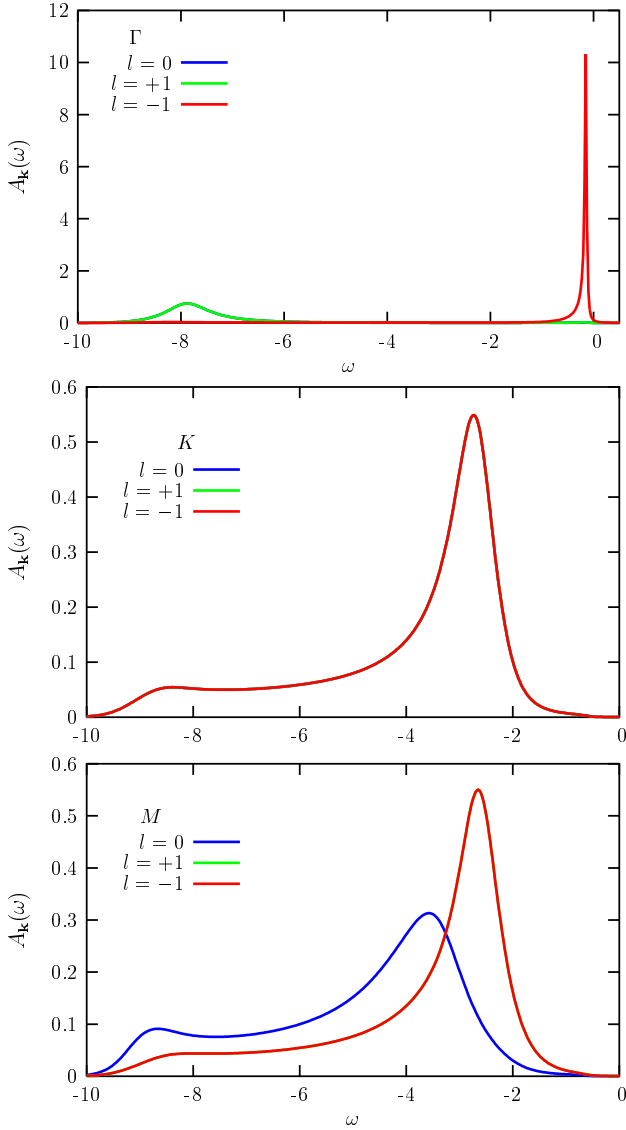


FIG. 6: (color online) Hole spectral function $A_{\mathbf{k}}(\omega)$ at the special MBZ points Γ , K , and M . Here $\Delta = 4$.

formally second-order structure of the self-energy correction. The quasiparticle (hole) energy is maximum (minimum) at the Γ point $\mathbf{k} = (0, 0)$ for $l = -1$, corresponding to BZ momentum $-\mathbf{Q}$.

Figure 6 shows the spectral function $A_{\mathbf{k}}(\omega)$ for the special points Γ , K , and M . The weak self-energy correction in the broadened lower band of the frustrated 120° ordered AF state results in no visible oscillatory structure, typically associated with the string of broken bonds as the hole moves in the AF background. As expected, the spectral function at the Γ point $\mathbf{k} = (0, 0)$ and $l = -1$ shows a coherent quasiparticle peak, as this state lies at the top of the lower band. All three branches are degenerate at point K , as at the HF level. The spectral functions at K and M points show well-defined peak structures, with finite quasiparticle damping as these states lie well within the band. The quasiparticle peak broadens and

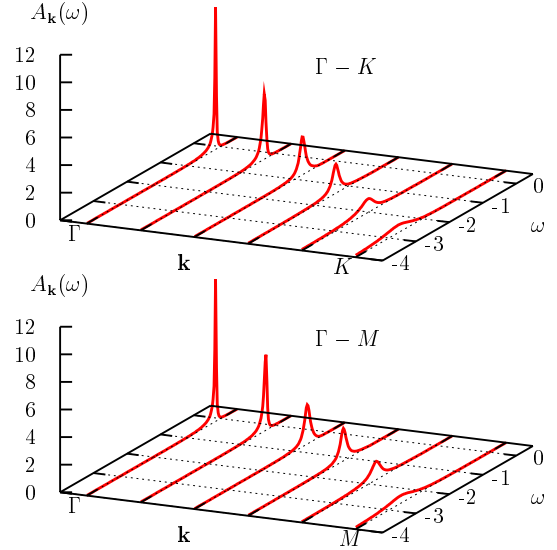


FIG. 7: (color online) Hole spectral function $A_{\mathbf{k}}(\omega)$ along the $\Gamma - K$ and $\Gamma - M$ directions for the lowest-energy branch $l = -1$.

loses intensity along both the $\Gamma - K$ and $\Gamma - M$ directions, as seen in Fig. 7.

B. Electron Dynamics (Upper Band)

Self-energy correction in the narrow upper band is relatively large and self consistency is noticeably slower (Fig. 8), illustrating the importance of multi-magnon processes and resulting in the characteristic oscillatory structure in the spectral functions (Fig. 10) associated with string states.

Figure 9 shows the quasiparticle dispersion along the $\Gamma - K - M - \Gamma$ directions for the lowest-energy branch $l = 0$. The lowest-energy state at point M shows a well-defined quasiparticle peak at $\omega = 1.3$, along with a long incoherent tail, as seen in Fig. 10. All branches are degenerate at K , second and third branches at M , first and second branches at Γ , while at $N = (2\pi/5, 0)$ all branches are non-degenerate, exactly as at the HF level.

The states K , Γ , and N , which are well inside the band, are strongly damped and yield dominantly incoherent spectral functions, along with small quasiparticle peaks at nearly same frequency $\omega \approx 2$ (Fig. 10). It is the strong negative peak in the self energy at $\omega \approx 2$ (Fig. 8) which leads to nearly same quasiparticle energy for all \mathbf{k} points, resulting in drastically reduced quasiparticle bandwidth (Fig. 9) and enhanced effective mass. Figure 11 shows that the well-defined quasiparticle peak at M rapidly diminishes in intensity and disappears as one moves along the $M - \Gamma$ direction. However, in the $M - K$ direction, the quasiparticle peak is discernible in the full k range. In the $K - \Gamma$ direction, the quasiparticle peak

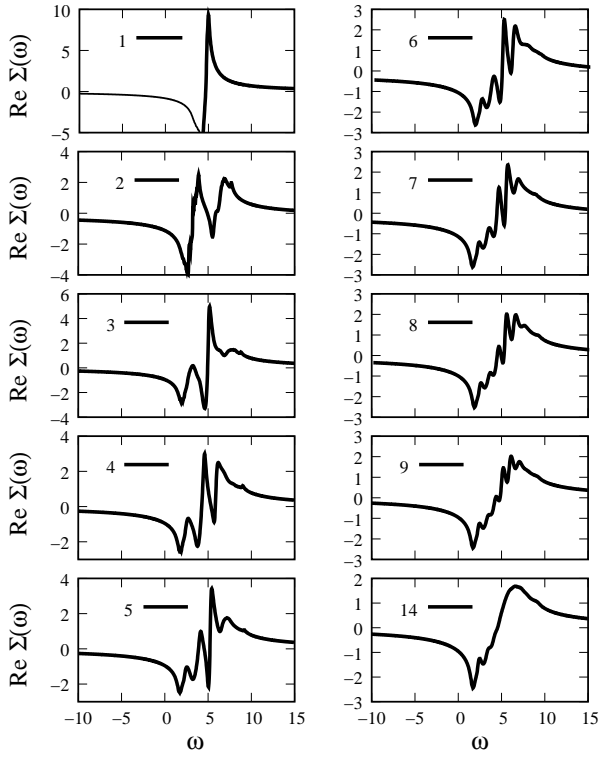


FIG. 8: Variation of electron self energy with iterations for the upper band, effectively illustrating the role of successively higher-order magnon processes. Here $\Delta = 4$ and $\mathbf{k} = (-\frac{2\pi}{3}, 0)$, $l = 0$.

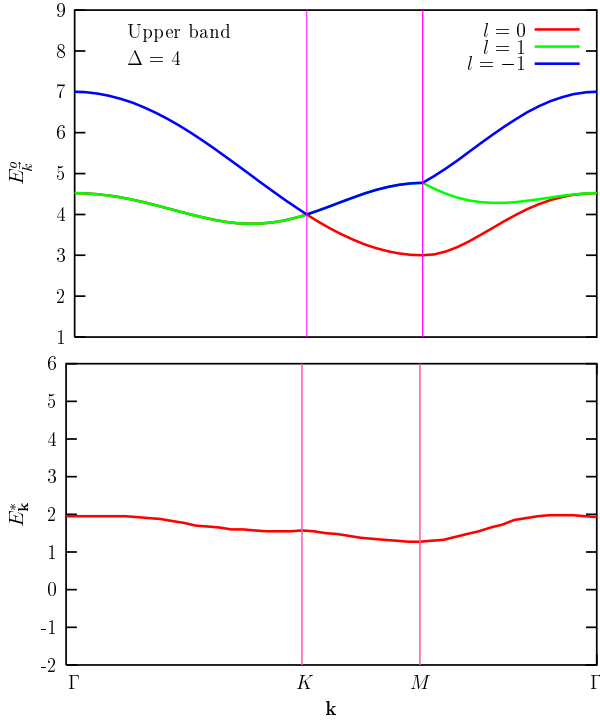


FIG. 9: (color online) Quasiparticle dispersion $E_{\mathbf{k}}^*$ for the lowest-energy branch $l = 0$ along different symmetry directions in the MBZ (lower panel), along with the HF dispersion $E_{\mathbf{k}}^0$ for comparison (upper panel).

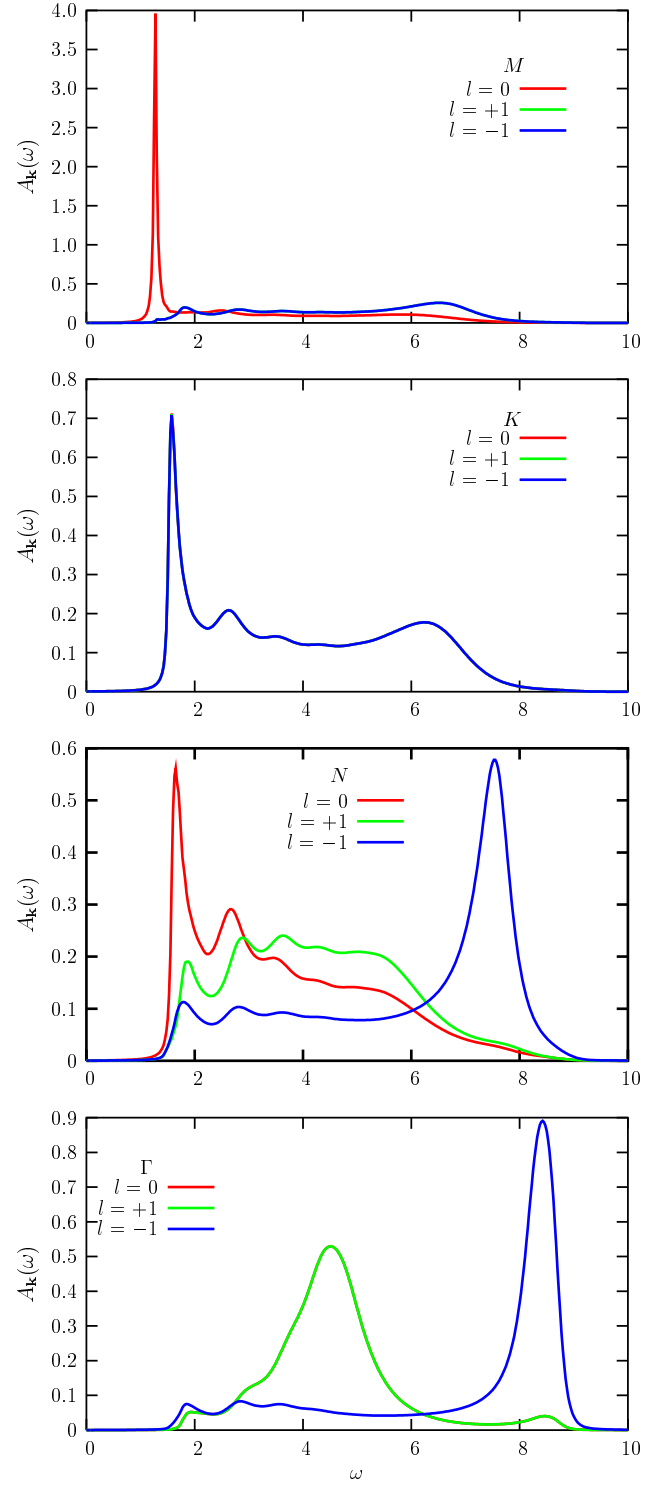


FIG. 10: (color online) Electron spectral function $A_{\mathbf{k}}(\omega)$ at the special MBZ points for $\Delta = 4$ ($U \approx 8.8$).

marginally increases and then rapidly disappears as one moves towards Γ .

The lowest-energy hole and electron pockets are shown in Fig. 12. The one-particle density of states is shown in Fig. 13 for $\Delta = 4$ and 3. The classical-level asymmetry strongly influences the quantum corrections and

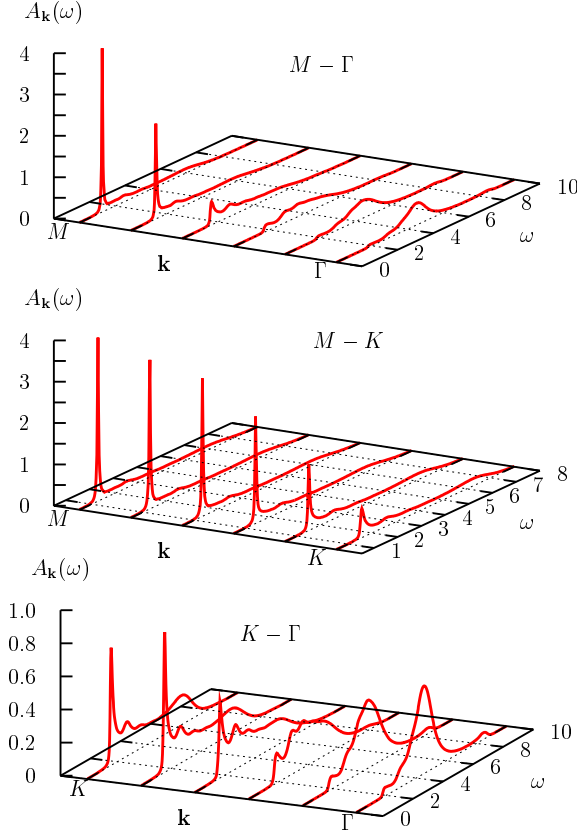


FIG. 11: (color online) Evolution of the electron spectral function for the lowest-energy branch $l = 0$ along different symmetry directions.

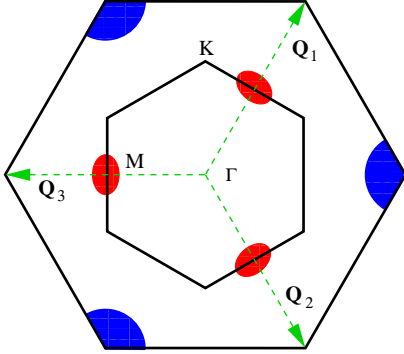


FIG. 12: (color online) Hole (blue) and electron pockets (red) corresponding to lowest-energy states in the Brillouin zone. $\mathbf{Q}_1, \mathbf{Q}_2, \mathbf{Q}_3$ are equivalent AF ordering wave vectors.

the characteristic signature of multi-magnon processes is dominant for the upper band corresponding to the narrow sharp peak at the classical level. As expected within the many-body expansion, the string-state signature of multi-magnon processes is more prominent for higher U . The renormalized gap vanishes for $U \approx 7$, whereas the HF band gap $2(\Delta - 2)$ vanishes at $U \approx 5$. The band gap is

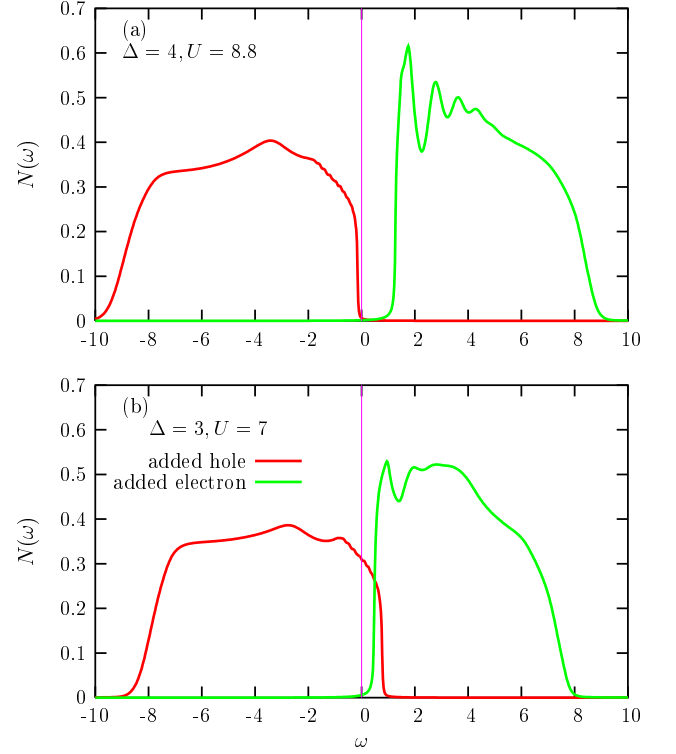


FIG. 13: (color online) Renormalised density of state for one added hole and electron for (a) $\Delta = 4$ and (b) $\Delta = 3$, showing the vanishing of energy gap.

indirect, with the lowest-energy hole and electron states corresponding to momenta $(4\pi/3, 0)$ and $(-2\pi/3, 0)$, respectively.

It is interesting to note that in the intermediate-coupling regime of interest, the interaction strength effectively controls the fermion-magnon scattering through three different aspects. With decreasing interaction strength, besides the explicit reduction in the fermion-magnon scattering matrix element due to U in Eq. (25), the classical-level fermion and magnon dispersions are also significantly modified. Due to enhanced virtual hopping and competition with the direct hopping term the sharp peak in the upper band DOS (Fig. 2) shifts towards higher energy. Also, the magnon energy ω_M at momentum $\mathbf{Q}/2$ decreases rapidly and vanishes at $\Delta = 2.9$.⁹ Fig. 13 shows the modifications in the upper band DOS due to these intermediate- U effects.

VI. CONCLUSIONS

In conclusion, we have studied the hole and electron dynamics in the 120° ordered AF state of the Hubbard model on a triangular lattice using a physically transparent fluctuation approach involving the dynamical spin fluctuations, which interpolates between the weak and strong coupling limits. Finite- U , double occupancy ef-

fects, neglected in earlier $t - J$ model studies, have been incorporated naturally in terms of classical level fermion and spin dynamics. Intrinsic features of the frustration-induced direct hopping dispersion associated with the 120° ordering - the broad flat band and the narrow sharp peak in the fermion DOS corresponding to lowest-energy hole and electron states - are characteristics of ferromagnetic and antiferromagnetic ordering, respectively. The qualitatively different self-energy corrections for hole and electron can therefore be conveniently visualized in terms of hole (electron) motion in an effective ferromagnetic (antiferromagnetic) spin background projected out of the 120° spin ordering.

For an added hole in the broad lower band, the reduced density of scattering states suppresses the fermion-magnon interaction resulting in nearly coherent quasiparticle peak for all \mathbf{k} states. No signature of string states in the spectral function reflects an effective F background seen by holes near the top of the lower band. Quasiparticle dispersion shows a nearly momentum-independent shift of hole energies, implying no mass renormalization.

For an electron in the lowest-energy branch $l = 0$ of the upper band, quasiparticle peak is observed only near the MBZ boundary ($M - K$), and rapidly vanishes away from it. Strong incoherent behaviour and clear signature of string states in the spectral function is a consequence of an effective AF background seen by electrons near the bottom of the upper band. The strong and nearly momentum-independent peak in the self energy leads to nearly same quasiparticle energy for all \mathbf{k} points, resulting in drastically reduced bandwidth and enhanced effective mass.

The renormalized band gap was found to vanish for $U \approx 7$, yielding a first-order M-I transition, as also obtained earlier for the frustrated square-lattice AF.¹⁴ On the other hand, for the unfrustrated AF the band gap never vanishes for any finite U . The vanishing of band gap at moderate U for both frustrated antiferromagnets due to frustration-induced band broadening thus highlights the role of frustration in M-I transition.

Finally, frustration and spin fluctuations are involved in an interesting interplay with respect to stability of the insulating state. Frustration generally enhances spin fluctuations and magnetic disordering. It will therefore be interesting to also examine the interband self-energy contribution which reduces magnetic order due to interband spectral weight transfer, and also widens the band gap and thereby stabilizes the insulating state. The first-order interband contribution exactly cancels for negligible AF bandwidth, as for the unfrustrated AF in the strong-coupling limit,¹⁴ but will survive for finite frustration-induced bandwidth, thus highlighting the interplay between frustration and spin fluctuations, and providing deeper insight into the nature of the Mott insulator.

APPENDIX: FERMION-MAGNON MATRIX ELEMENT IN THE STRONG-COUPLING LIMIT

We show that to leading order in the $U/t \rightarrow \infty$ limit, the intraband fermion matrix elements reduce to order t/Δ , and the fermion-magnon matrix element explicitly reduces to order t , as within the $t - J$ model.

For the magnon energy and magnon amplitudes in the y' and z' directions we have

$$\begin{aligned}\omega_{\mathbf{q}} &= 3JS[(1 - \gamma_{\mathbf{q}})(1 + 2\gamma_{\mathbf{q}})]^{1/2} \\ \mathcal{Y}_{\mathbf{q}}^2 &= \frac{3JS}{4\omega_{\mathbf{q}}}(1 + 2\gamma_{\mathbf{q}}) \\ \mathcal{Z}_{\mathbf{q}}^2 &= \frac{3JS}{4\omega_{\mathbf{q}}}(1 - \gamma_{\mathbf{q}})\end{aligned}\quad (\text{A.1})$$

$$\text{where } \gamma_{\mathbf{q}} = \frac{1}{3} \left[\cos q_x + 2 \cos \frac{q_x}{2} \cos \frac{\sqrt{3}}{2} q_y \right].$$

For the lower (-) and upper (+) bands, the fermion amplitudes given in Eq. (11) reduce to

$$\alpha_{\mathbf{k}}^{\mp} \simeq \pm \frac{1}{\sqrt{2}} \left(1 \pm \frac{\xi_{\mathbf{k}}}{2\Delta} \right), \quad \beta_{\mathbf{k}}^{\mp} \simeq + \frac{1}{\sqrt{2}} \left(1 \mp \frac{\xi_{\mathbf{k}}}{2\Delta} \right). \quad (\text{A.2})$$

Hence in terms of the spin raising and lowering operators defined below, the intraband fermion matrix elements

$$\begin{aligned}\langle \sigma^+ \rangle &\equiv \langle \mathbf{k}, l | \sigma_{z'} + i\sigma_{y'} | \mathbf{k} - \mathbf{q}, m \rangle \simeq \frac{\xi_{\mathbf{k},l}}{\Delta} \\ \langle \sigma^- \rangle &\equiv \langle \mathbf{k}, l | \sigma_{z'} - i\sigma_{y'} | \mathbf{k} - \mathbf{q}, m \rangle \simeq \frac{\xi_{\mathbf{k}-\mathbf{q},m}}{\Delta}\end{aligned}\quad (\text{A.3})$$

for lower band states are explicitly of order t/U .

In terms of corresponding magnon amplitudes

$$\Phi_{\mathbf{q},\lambda}^{\pm} \equiv \sqrt{3} [| \mathbf{q}, \lambda \rangle_{z'} \pm i | \mathbf{q}, \lambda \rangle_{y'}] = \mathcal{Z}_{\mathbf{q},\lambda} \pm \mathcal{Y}_{\mathbf{q},\lambda} \quad (\text{A.4})$$

for the advanced mode, the fermion-magnon matrix element

$$\begin{aligned}\sqrt{3}M &= U[-i\langle \sigma_{y'} \rangle \mathcal{Y} + \langle \sigma_{z'} \rangle \mathcal{Z}] \\ &= U[\langle \sigma^+ \rangle \Phi^- + \langle \sigma^- \rangle \Phi^+]/2 \\ &= -(\xi_{\mathbf{k},l} - \xi_{\mathbf{k}-\mathbf{q},m})\mathcal{Y}_{\mathbf{q},\lambda} + (\xi_{\mathbf{k},l} + \xi_{\mathbf{k}-\mathbf{q},m})\mathcal{Z}_{\mathbf{q},\lambda} \\ &= \xi_{\mathbf{k},l}\Phi_{\mathbf{q},\lambda}^- + \xi_{\mathbf{k}-\mathbf{q},m}\Phi_{\mathbf{q},\lambda}^+ \quad (\text{where } m = l - \lambda)\end{aligned}\quad (\text{A.5})$$

explicitly reduces to order t .

The above expression for the fermion-magnon matrix element has exactly same structure as the result $\sqrt{3}tM(k, q) = \sqrt{3}t[v_{\mathbf{q}}h_{\mathbf{k}} - u_{\mathbf{q}}h_{\mathbf{k}+\mathbf{q}}]$ obtained within the $t - J$ model.¹⁷ Indeed, magnon amplitudes $u_{\mathbf{q}}$ and $v_{\mathbf{q}}$ in Ref. [17] exactly correspond to $\mathcal{Z}_{\mathbf{q}} \pm \mathcal{Y}_{\mathbf{q}}$, and $(\sqrt{3}t)h_{\mathbf{k}} \equiv \sqrt{3}t \sum_{\delta} \sin \mathbf{k} \cdot \hat{\delta} = -\xi_{\mathbf{k}-\mathbf{Q}}$. However, the Goldstone-mode contribution appears to be different. While our

fermion-magnon matrix element vanishes for the Goldstone mode $q \rightarrow 0$, $\lambda = 0$, for which $\gamma_{\mathbf{q}} \rightarrow 1$ and the magnon amplitude $\mathcal{Z} \rightarrow 0$ representing rigid spin rotation about z axis, the matrix element $M(\mathbf{k}, \mathbf{q})$ in Ref. [17] does not vanish. The other two Goldstone modes $q \rightarrow 0$, $\lambda = \pm 1$, for which $\gamma_{\mathbf{q}} \rightarrow -1/2$ and $\mathcal{Y} \rightarrow 0$,

do yield non-vanishing matrix elements with $M^2 \sim 1/q$, although resulting in a finite contribution $\int q dq/q$ from long-wavelength modes. Thus, for the triangular-lattice AF, long-wavelength modes do contribute to the fermion-magnon scattering.

* Electronic address: psriv@iitk.ac.in

† Electronic address: avinas@iitk.ac.in

¹ K. Kanoda, *Physica C* **282-287**, 299 (1997); K. Kanoda, *Hyperfine Interact.* **104**, 235 (1997).

² R. H. McKenzie, *Science*, **278**, 820 (1997).

³ K. Takada *et al.*, *Nature* **422**, 53 (2003).

⁴ H. H. Weitering, X. Shi, P. D. Johnson, J. Chen, N. J. Dinardo, and S. Kempa, *Phys. Rev. Lett.* **78**, 1331 (1997).

⁵ T. Inami, Y. Ajiro, and T. Goto, *J. Phys. Soc. Jpn.* **65**, 2374 (1996).

⁶ L. E. Svistov, A. I. Smirnov, L. A. Prozorova, O. A. Petrenko, L. N. Demianets, and A. Ya. Shapiro, *Phys. Rev. B* **67** 094 434 (2003).

⁷ O. P. Vajk, M. Kenzelmann, J. W. Lynn, S. B. Kim, and S.-W. Cheong, *cond-mat/0502006* (2005).

⁸ S. Ghosh and A. Singh, *cond-mat/0506475*.

⁹ A. Singh, *Phys. Rev. B* **71**, 214406 (2005).

¹⁰ Y. Shimizu, K. Miyagawa, K. Kanoda, M. Maesato, and G. Saito, *Phys. Rev. Lett.* **91**, 107001 (2003).

¹¹ F. Kagawa, T. Itou, K. Miyagawa, and K. Kanoda, *Phys. Rev. B* **69**, 064 511 (2004); F. Kagawa, T. Itou, K. Miya-

gawa, and K. Kanoda, *cond-mat/0409437* (2004).

¹² H. Morita, S. Watanabe, and M. Imada, *J. Phys. Soc. Jpn.* **71**, 2109 (2002).

¹³ M. Imada, T. Mizusaki, and S. Watanabe, *cond-mat/0307022* (2003).

¹⁴ P. Srivastava and Avinash Singh, *Phys. Rev. B*, **70**, 115103 (2004).

¹⁵ A. Singh and P. Goswami, *Phys. Rev. B* **66**, 92402 (2002).

¹⁶ L. Capriotti, A. E. Trumper and S. Sorella, *Phys. Rev. Lett.*, **82**, 3899 (1999)

¹⁷ M. Azzouz and T. Dombre, *Phys. Rev. B*, **53**, 402 (1996).

¹⁸ A. E. Trumper, C. J. Gazza and L. O. Manuel, *Phys. Rev. B*, **69**, 184407 (2004).

¹⁹ W. Apel, H.-U. Everts and U. Körner, *Eur. Phys. J. B*, **5**, 317 (1998).

²⁰ Matthias Vojta, *Phys. Rev. B* **59**, 6027 (1999).

²¹ M. Vojta, E. Dagotto, *Phys. Rev. B*, **59**, 713 (1999).

²² M. C. Refolio, J. M. López Sancho, and J. Rubio, *cond-mat/0103459* (2001).